Acta Polytechnica CTU Proceedings **42**:77–82, 2023
https://doi.org/10.14311/APP.2023.42.0077

Published by the Czech Technical University in Prague

HIGH-SPEED X-RAY RADIOGRAPHY FOR EXPERIMENTS IN IMPACT DYNAMICS USING HIGH-POWER X-RAY TUBE, CESIUM IODINE SCINTILLATOR AND LABORATORY OPTICAL CAMERA

Jan Šleichrt*, Jan Falta, Tomáš Fíla

Czech Technical University in Prague, Department of Mechanics and Materials, Faculty of Transportation Sciences, Konviktská 20, 110 00 Prague 1, Czech Republic

* corresponding author: sleichrt@fd.cvut.cz

Abstract. X-ray radiography and computed tomography have become well-established methods for investigation of internal structure of objects and for defectoscopy. Recently, the methods have even been used for in-situ analysis of materials under mechanical loading. Although the techniques would be very suitable for analysis during dynamic events, their application is constrained by typical achievable frame rates. Therefore, fast imaging is usually limited to facilities providing sufficient flux like particle accelerators. In this paper, we test imaging performance of a laboratory-based setup with a high-power X-ray tube, a scintillation panel, and an optical camera. Fast-rotating object and typical specimens for impact testing are irradiated with different power settings and quality of captured images is evaluated and analyzed. It is found out that the system can be successfully used for imaging at several hundred frames per second allowing for inspection of slow impact dynamics experiments.

Keywords: High-speed X-ray radiography, scintillator, high-speed camera, impact dynamics.

1. Introduction

X-ray imaging is an experimental technique allowing for visualization of the internal structure of the irradiated objects. In engineering applications, the technique of planar X-ray radiography is well-established for defectoscopy, identification of internal imperfections, or control of manufacturing processes. Typically, an X-ray detector working on a flat panel or direct conversion principle is currently used to capture the planar X-ray images, or even volumetric computed tomography reconstruction of stationary objects in very high resolution (voxel size corresponding to units of micrometers) [1]. In-situ investigation of slowly moving objects (typically stop-and-go inspection on a conveyor during manufacturing process) or objects subjected to quasi-static mechanical loading is also ordinarily possible [2, 3]. Although the method would be perfectly suitable even for in-situ analysis of the internal structure of materials subjected to dynamic processes, like impact or vibration, such applications are still extremely rare in laboratory or field environments as the frame rate of conventional X-ray detectors is not sufficient. The problem can be overcome using particle accelerators or flash X-ray systems providing sufficient photon flux for better imaging performance of scintillation panels in combination with high-speed cameras [4–6]. However, this comes with disadvantages regarding the costs, system complexity, accessibility, flexibility, constraints in image resolution, statistics, and size of the object. Recently, state-of-the-art detectors using direct deposition technology allowing for high frame rates have been introduced, but still exhibit high costs, low scalability, and limited size [7]. In this paper, we introduce a system for high-speed X-ray radiography of transient events consisting of a conventional high-power X-ray tube, large area scintillation panel, and a variety of optical cameras (including costly high-speed cameras as well as budget scientific or standard cameras). The imaging performance of the system is tested exhibiting superiority in achievable frame rates over standard radiation imaging detectors and allowing for successful imaging of transient dynamic processes. The advantages and disadvantages of the system are discussed as well.

2. Materials and methods

2.1. Imaging principle

An observed object is irradiated by a beam of an X-ray emitting source. After penetration through the object, the X-ray beam hits the scintillation panel, which is in principle a thin luminescent layer producing visible light when excited by ionizing radiation. The visible light image produced by the scintillation panel is then captured using a laboratory optical camera. The measurement principle is shown in Figure 1. This arrangement requires aligning the camera with the axis of the X-ray beam. Ionizing radiation hitting the CMOS chip elements of the camera causes randomly distributed high-saturated "bright" pixels, so-called zingers. This unsolicited noise has a significant effect on image quality and should be prevented, minimized, or filtered [8]. In our case, signal intensity (and thus maximum imaging speed) is prioritized to image quality. Therefore, zingers are widely present in the images and are filtered during post-processing by a simple median filter at the cost of reduction in

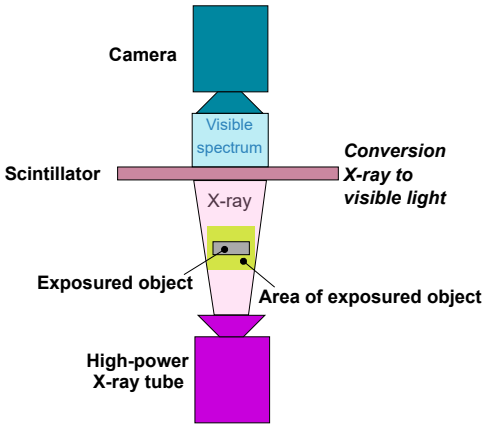

Figure 1. X-ray imaging principle.

detail detectability.

2.2. X-ray tube

Irradiation was performed by an MXR-225HP/11 X-ray tube (Comet AG, Switzerland). This high-power X-ray tube has a tungsten target and dual focal spot capability providing spot size of 1 mm at maximum power of 1 800 W in the large spot mode and 0.4 mm at maximum power of 800 W in the small spot mode. The generated beam is approximately conical with angular span of 30–40°. Acceleration voltage can be set in range of 50–225 kV providing sufficient penetration through objects with medium size and density (penetrated thickness corresponding to several centimetres of light metals and alloys).

2.3. Scintillation panel

The conversion of emitted photons from the X-ray tube to the visible-light spectrum was performed by the Cesium Iodine (CsI) Scintillation panel – GPXS J10666 (Hamamatsu Photonics, Japan) based on the luminescence effect. Physical dimensions of the panel are $500 \times 500\,\mathrm{mm}^2$ with effective active area of $450 \times 450\,\mathrm{mm}^2$. This large-format panel combines the advantages of a low after-glow effect and high relative light output with its maximum intensity peak lying in wavelength range of 400–600 nm.

2.4. Laboratory optical camera

A standard laboratory camera Kiralux CS135MUN (Thorlabs, USA) with a monochromatic 10-bit CMOS chip was used together with a standard C-Mount camera lens MVL6WA (Thorlabs, USA) with a fixed focal length of 6 mm, minimum focal distance of 200 mm and maximum aperture of f/1.4. The camera was operated using generic software provided by the manufacturer with the images grabbed directly to a PC hard drive using its USB3.0 interface. The chip has a full frame resolution of 1280×1024 px with pixel size of $4.8 \times 4.8\,\mu\mathrm{m}^2$ and maximum quantum efficiency of 60 % at 600 nm matching with the typical wavelength of light emitted by the scintillation panel. The camera can operate at 165.5 fps with full frame images and supports chip windowing, binning and amplification while its maximum imaging speed is 6 712 fps at resolution of 16×2 px. Besides the Kiralux camera, two other cameras were used: Sony Cyberhot RX100 IV (Sony Corporation, Japan) representing a non-scientific budget equipment and Photron SA-Z ultra high-speed camera (Photron, Japan). Typical performance of these two cameras is briefly discussed in Section 4 for illustrative purposes only. Although the Photron SA-Z high-speed camera is available to the authors and can provide significantly better performance, it was intentionally used only for demonstration and in-depth analysis of the ultra high-speed camera results is considered beyond scope of this study. More importantly, long-term exposure to high-intensity radiation can potentially damage extremely costly equipment. Therefore, performance that can be reached using an affordable camera is demonstrated instead.

2.5. Experiment

The experimental program was divided into two main parts: i) investigation of full-beam intensities and image quality of typical specimens in stationary position with a variety of X-ray tube and imaging camera settings, and ii) imaging of fast rotating object. The experimental setup was composed of the high-power X-ray tube, a sample holder – tripod, the scintillation panel, and the laboratory optical camera. The individual components were axis-aligned (see Figure 1). Typically, the X-ray tube was operated with an output power of 1 500 W, although its maximum output power rating is 1 800 W. The tube has, however, a limited lifetime at the maximum output power and therefore most of the imaging was performed at the maximum continuous power settings. Several objects representing typical specimens for impact dynamic experiments were irradiated, namely: closed-cell aluminium foam (cylinder with approximate dimensions of 60 mm in diameter and 30 mm in height, or larger integral blocks), additively manufactured stainless steel auxetic lattice filled with a polymeric filling (cube with approximate dimensions of $12 \times 12 \times 12\,\mathrm{mm}^3$), additively manufactured aluminium alloy auxetic lattice (cube with approximate dimensions of $14 \times 14 \times 14\,\mathrm{mm}^3$) [9, 10]. A CPU cooling fan including its aluminum cooler chassis was used as a fast-rotating object while a single blade of the fan was covered by lead to increase imaging contrast. The fan was rotated at a constant angular velocity of approx. 17 RPS with peripheral speed of approximately $3.5\,\mathrm{m\,s}^{-1}$ at the end of fan's blade. The X-ray images were captured using different settings of the camera and the X-ray tube to optimize for image quality and speed. Various settings of frame rate, exposure time, binning, gain, X-ray voltage and power were used during the experiments to improve contrast and image statistics at a given frame rate. The experiments were performed in an X-ray bunker shielded with high density concrete blocks doped with

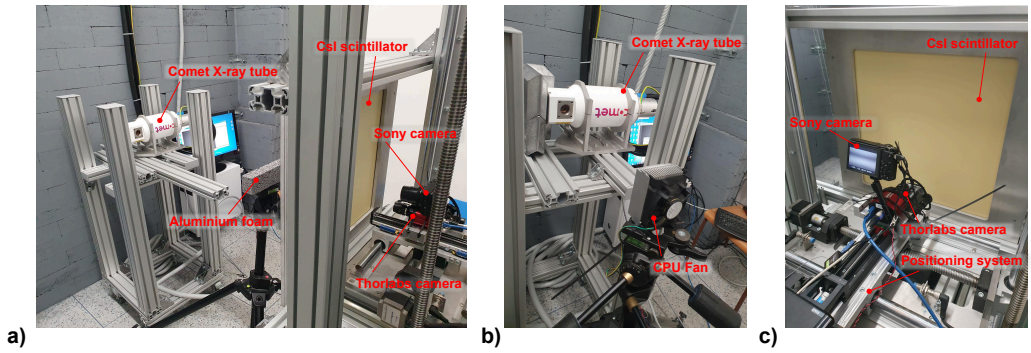

FIGURE 2. Experimental setup: (a) an entire experimental setup with an aluminium foam in front of the X-ray tube; (b) CPU fan with aluminium cooler in front of the X-ray tube; and (c) cameras behind the scintillator.

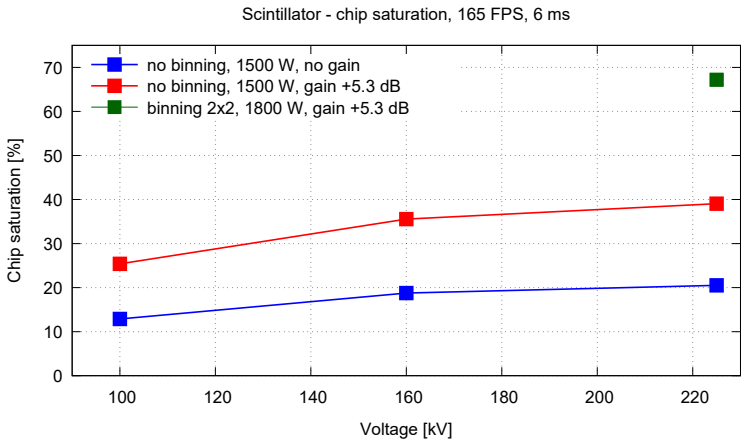

FIGURE 3. Average flat field intensities expressed as a fraction of chip's saturation recorded at 165 fps using an exposure time of 6 ms. The distance between the X-ray tube and the scintillator was 1 060 mm and between the scintillator and the camera 150 mm.

iron ore. Lights in the bunker were turned off during the imaging process to measure output of the scintillator unaffected by ambient light conditions. Resolution of the system was limited primarily by the focal spot size of the X-ray tube (1 mm for maximum power of 1 800 W, 0.4 mm for power of up to 800 W) and by thickness of the active layer of the scintillator of 0.4 mm. In general, details smaller than focal spot size or length of tangential projection through the scintillation layer can be only hardly detected. On the other hand, resolution of the camera images was much higher even for settings with binning and windowing as it was around 0.2 mm in the worst case. The experimental setup showing arrangement with a stationary object as well as with the CPU fan is shown in Figure 2.

3. RESULTS

3.1. FULL BEAM INTENSITY

Full beam images (i.e., images of the irradiated scintillation panel when no object is placed in the X-ray beam) were taken for different settings of the X-ray tube and the camera. Image noise and dark image values were evaluated and, in the worst case, both were approximately as high as 3 % of chip's saturation range (10-bit). Based on a common practice requiring a minimal signal-to-noise ratio (SNR) of 10 dB for the darkest part of the object (i.e., approx. 8 % of the chip's range above dark values) and at least the same range of 10 dB between the darkest part of the image and bright full beam background (i.e., approx. 25 % above dark values), it was estimated that full beam intensity has to reach at least approximately 30 % of the chip's range to provide minimal required image quality. Recorded average full beam intensities at 165 fps (exposure time of 6 ms) with a distance of the scintillator from the X-ray focal spot 1060 mm are shown in Figure 3. The distance of the camera from the scintillator was kept at approx. 150 mm for all the tests. This distance is lower than the minimum object distance of the lens, therefore an extension element was used to reduce it. Depending on the X-ray tube voltage and camera settings (pixel binning and signal amplification), the imaging performance can be investigated revealing that the required intensity is not reached without amplification or binning. However, as the intensity is linearly dependent on the exposure time, it can be expected that, for certain settings (gain of +5.3 dB, binning of at least 2×2), proportionally higher frame rates can be reached while still fulfilling the minimal required image quality.

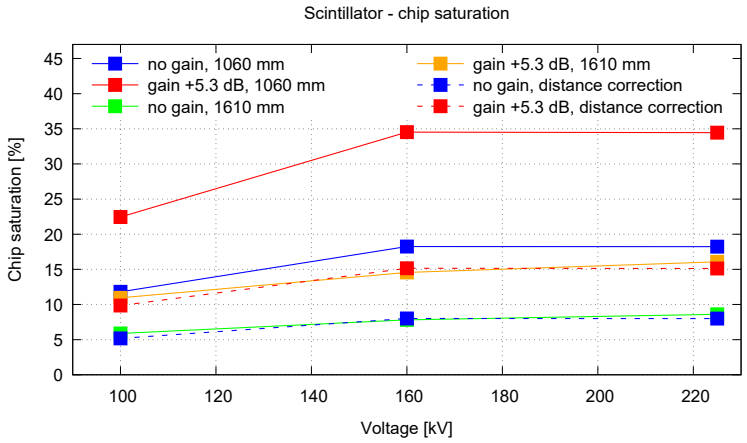

Figure 4. Average intensities of full beam images for two distances of the scintillator from the X-ray tube. Dashed lines represent an extrapolation of the measured values from 1 060 mm to a distance of 1 610 mm fulfilling the inverse-square law.

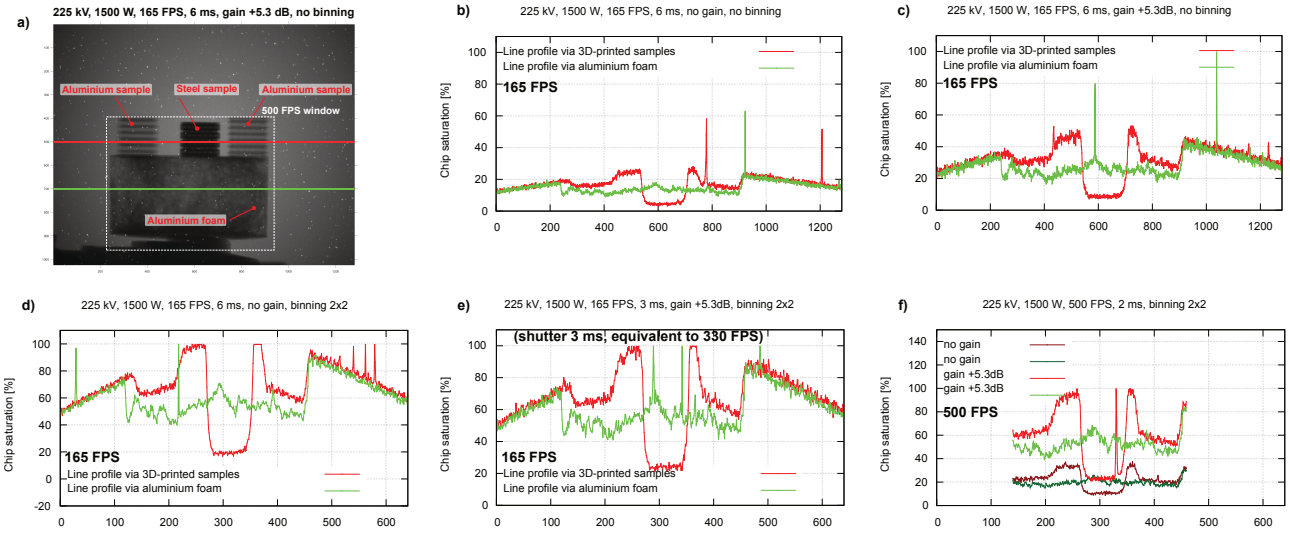

Figure 5. Intensity line profiles through typical specimens at different camera settings; (a) X-ray image; (b)-(d) 165 fps; (e) shutter speed for 330 fps; (f) 500 fps.

3.2. Intensity with distance

The expected behavior of intensity according to the inverse-square law (quadratic decrease of intensity with distance) was confirmed by placing the scintillation panel at two distances from the X-ray focal spot. The first distance was 1 060 mm and the second distance was 1 610 mm. Average intensities of full beam images for both distances at different settings of the X-ray tube are shown in Figure 4. Dashed lines represent the values from 1 060 mm extrapolated to a distance of 1 610 mm using the inverse-square law showing good correlation with the measured values. Note that the recorded intensities for 1 060 mm do not perfectly match the values in Figure 3. Because of the open installation of the scintillator, its maximum light output deteriorated over time during long term exposure to excessive radiation. Effects of long term after-glow, ghosting, and non-stable scintillator output (caused by dust accumulation etc.) were present. In general, the lifetime of scintillator is usually extremely sensitive to radiation exposure and the environmental conditions. However, the effects observed during this study were temporary and the scintillator restored approximately its initial performance after some time (couple of hours to days).

3.3. Typical specimens

Intensity line profiles were used as a tool to investigate image quality. Representative X-ray image of typical specimens including the closed-cell metal foam stacked together with the additively manufactured lattices made of stainless steel and aluminum alloy as well as line profiles corresponding to different camera settings are shown in Figure 5. Recorded intensities in most of the cases fulfilled the requirements summarized in the previous Section 3.2 while images with frame rates of up to 500 fps with reasonable quality were captured. With application of binning, intensities close to saturation of the chip were reached in Figure 5d (165 fps, no gain, binning 2×2, exposure time 6 ms). Figure 5e represents an image where a

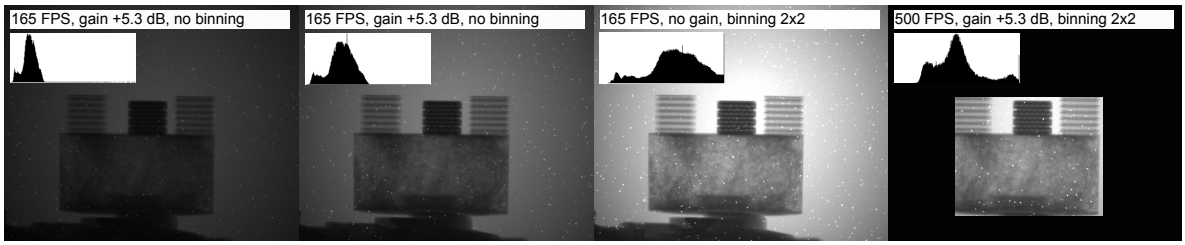

FIGURE 6. X-ray images of the typical specimens taken at 225 kV and 1 500 W with different camera settings including their histograms normalized to full range of the chip. The images from left to right correspond to the line profiles (b), (c), (d) and (f) in Figure 5.

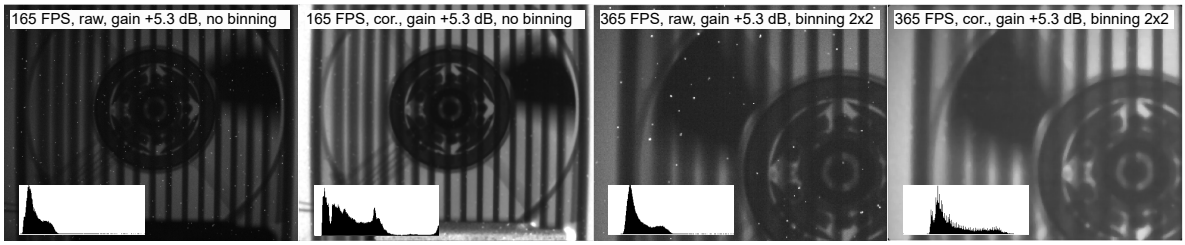

FIGURE 7. CPU fan rotating at approx. 17 RPS recorded at two different frame rates. Raw images and images after corrections are shown including their histograms normalized to the full range of the chip.

gain of +5.3 dB was added to the settings of Figure 5d. Shutter time was reduced to 3 ms to prevent overexposure. The resulting image is therefore equivalent to frame rate of 330 fps. As it is not possible to reach this frame rate without windowing, the full-frame image with binning was taken at 165 fps to allow for direct comparison with the image in Figure 5d. Increase in image statistics and contrast at a cost of higher noise, lower resolution and smaller active area is apparent in Figure 5f. Corresponding X-ray images of the typical specimens taken with different settings are shown in Figure 6 including histograms normalized to full range of the chip.

3.4. Rotating CPU fan

Typical images of the CPU fan rotating at constant angular velocity of approx. 17 RPS captured at frame rate of 165 fps and 365 fps are shown in Figure 7. Raw uncorrected images and images after dark field, flat field correction (normalization using full beam images), and removal of zingers using a median filter are compared including histograms. The image quality at both frame rates allows for tracking of the fan and motor pole's position and is considered suitable for subsequent image processing and analysis. Motion blur effect caused by peripheral velocity of the fan of approx. 3.5 m s^{-1} is apparent in the images at both frame rates, requiring post-processing techniques of blur removal to perform more complex analysis of the moving fan itself. Based on the X-ray tube focal spot size of 1 mm, it is estimated that the velocity limit not requiring post-processing of blur effects is approx. 0.16–0.50 m s^{-1} which is, together with the achieved frame rates, suitable for dynamic testing at low and intermediate strain rates.

4. Discussion

4.1. Advantages and disadvantages

Based on the performed experimental work and the acquired results, the advantages and disadvantages of the used system for high-speed X-ray imaging in impact dynamics can be summarized. The main advantages are formulated in the following points: relative affordability of the individual components, versatile laboratory-based system, very high frame rates in comparison with standard radiation imaging detectors, the flexibility of the system that can be application optimized using different optics, cameras, geometry, field of views, etc. with low costs of the upgrade. On the other hand, the limitations lay in relatively low image resolution, small pixels of the optical cameras reducing imaging efficiency, the complexity of the system composed of many elements, radiation harm to cameras, obligatory use of windowing, binning, and amplification for increasing frame rates, and low energy resolution. Performance of the system can be significantly improved by the high-speed camera (Photron SA-Z) as the results of similar image quality were possible at frame rates of 1–2 kfps (see an illustrative image in Figure 8a) because of the significantly higher sensitivity of the chip. On the other hand, still, acceptable results could be achieved even with the budget Sony Cybershot RX100 IV at 240 fps (illustrative image in Figure 8b).

4.2. Application potential

The achieved results indicate that the system is capable of high-speed X-ray imaging of impact dynamics experiments performed at low and intermediate strain rates and can provide acceptable frame rate, resolution, and image detail. The system will be

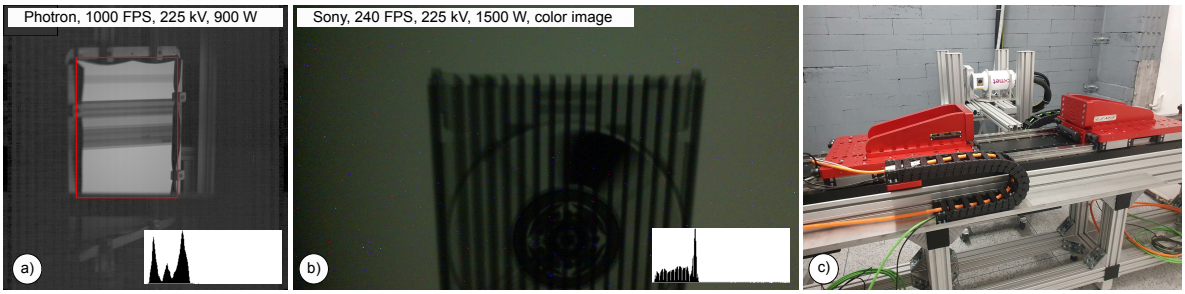

Figure 8. a) Hollow aluminum profile with cross-section of $180 \times 90\,\mathrm{mm}^2$ captured using Photron SA-Z high-speed camera at 1 000 fps (225 kV, 900 W). The image was taken using a mirror behind the scintillator to prevent direct irradiation of the Photron camera. The frame of the mirror is visible around the X-ray projection highlighted by red rectangle; (b) rotating CPU fan captured using Sony Cybershot RX100 IV at 240 fps (225 kV, 1 500 W); (c) dynamic testing device with linear motors installed in the X-ray imaging setup.

used together with an in-house developed dynamic testing device with linear motors allowing for precisely controlled and time-synchronized experiments with impact velocities of 0–8 $\mathrm{m\,s^{-1}}$ and typical impact forces up to 5 kN. The potential research fields include crack propagation, fracture and failure, lattice collapse, internal damage, or strain rate-sensitive filling materials. The dynamic testing device with linear motors installed within the X-ray imaging setup is shown in Figure 8c.

5. Conclusions

The performance of high-speed X-ray imaging system using large area CsI scintillation panel and the affordable scientific optical camera was investigated through series of experiments analyzing its application potential for continuous X-ray radiography in impact dynamics. It was concluded that the system could be used for imaging of dynamic impact events conducted at low and intermediate strain rates with acceptable image quality.

Acknowledgements

The research was supported by the Czech Science Foundation (project Junior Star no. 22-18033M).

References

[1] J. Dudak. High-resolution X-ray imaging applications of hybrid-pixel photon counting detectors Timepix. *Radiation Measurements* **137**:106409, 2020. https://doi.org/10.1016/j.radmeas.2020.106409

[2] P. Koudelka, T. Fila, V. Rada, et al. In-situ X-ray differential micro-tomography for investigation of water-weakening in quasi-brittle materials subjected to four-point bending. *Materials* **13**(6):1405, 2020. https://doi.org/10.3390/ma13061405

[3] D. Vavrik, P. Benes, T. Fila, et al. Local fracture toughness testing of sandstone based on X-ray tomographic reconstruction. *International Journal of Rock Mechanics and Mining Sciences* **138**:104578, 2021. https://doi.org/10.1016/j.ijrmms.2020.104578

[4] X. Zhai, Z. Guo, J. Gao, et al. High-speed X-ray visualization of dynamic crack initiation and propagation in bone. *Acta Biomaterialia* **90**:278–286, 2019. https://doi.org/10.1016/j.actbio.2019.03.045

[5] E. Strassburger, S. Bauer, S. Weber, H. Gedon. Flash X-ray cinematography analysis of dwell and penetration of small caliber projectiles with three types of SiC ceramics. *Defence Technology* **12**(3):277–283, 2016. https://doi.org/10.1016/j.dt.2016.01.011

[6] S. Moser, M. Wickert, S. Nau. High-speed X-ray imaging and 3D analysis of impact-formed fragments. In M. Versluis, E. Stride (eds.), *32nd International Congress on High-Speed Imaging and Photonics*, vol. 11051, p. 110510O. SPIE, 2019. https://doi.org/10.1117/12.2525447

[7] D. Vavrik, J. Dudak, I. Kumpova, J. Zemlicka. Application of 2 × 5 MPX3 camera with monolithic sensor for phase contrast imaging and computed tomography. *Journal of Instrumentation* **17**(03):C03020, 2022. https://doi.org/10.1088/1748-0221/17/03/c03020

[8] J. Mertens, J. Williams, N. Chawla. A method for zinger artifact reduction in high-energy X-ray computed tomography. *Nuclear Instruments and Methods in Physics Research Section A: Accelerators, Spectrometers, Detectors and Associated Equipment* **800**:82–92, 2015. https://doi.org/10.1016/j.nima.2015.08.012

[9] T. Fila, P. Koudelka, J. Falta, et al. Impact behavior of additively manufactured stainless steel auxetic structures at elevated and reduced temperatures. *Advanced Engineering Materials* **23**(1):2000669, 2020. https://doi.org/10.1002/adem.202000669

[10] J. Sleichrt, T. Fila, P. Koudelka, et al. Dynamic penetration of cellular solids: Experimental investigation using Hopkinson bar and computed tomography. *Materials Science and Engineering: A* **800**:140096, 2021. https://doi.org/10.1016/j.msea.2020.140096